Lock-in and quasiperiodicity in hydrodynamically self-excited flames: Experiments and modelling

Larry K.B. Li[*], Matthew P. Juniper

Department of Engineering, University of Cambridge, Trumpington Street, Cambridge CB2 1PZ, UK

Available online 26 September 2012

Abstract

Hydrodynamically self-excited flames are often assumed to be insensitive to low-amplitude external forcing. To test this assumption, we apply acoustic forcing to a range of jet diffusion flames. These flames have regions of absolute instability at their base and this causes them to oscillate at discrete natural frequencies. We apply the forcing around these frequencies, at varying amplitudes, and measure the response leading up to lock-in. We then model the system as a forced van der Pol oscillator.

Our results show that, contrary to some expectations, a hydrodynamically self-excited flame oscillating at one frequency is sensitive to forcing at other frequencies. When forced at low amplitudes, it responds at both frequencies as well as at several nearby frequencies, indicating quasiperiodicity. When forced at high amplitudes, it locks into the forcing. The critical forcing amplitude for lock-in increases both with the strength of the self-excited instability and with the deviation of the forcing frequency from the natural frequency. Qualitatively, these features are accurately predicted by the forced van der Pol oscillator. There are, nevertheless, two features that are not predicted, both concerning the asymmetries of lock-in. When forced below its natural frequency, the flame is more resistant to lock-in, and its oscillations at lock-in are stronger than those of the unforced flame. When forced above its natural frequency, the flame is less resistant to lock-in, and its oscillations at lock-in are weaker than those of the unforced flame. This last finding suggests that, for thermoacoustic systems, lock-in may not be as detrimental as it is thought to be.
© 2012 The Combustion Institute. Published by Elsevier Inc. All rights reserved.

Keywords: Absolute instability; Combustion instability; Global instability; Thermoacoustic instability

1. Introduction

In the analysis of thermoacoustic systems, a flame is usually characterised by the way its heat release responds to acoustic forcing. This response depends on the hydrodynamic stability of the flame. Some flames, such as a premixed bunsen flame, are hydrodynamically globally stable. They respond only at the forcing frequency. Other flames, such as a jet diffusion flame, are hydrodynamically globally unstable. They oscillate at their own natural frequencies and are often assumed to be insensitive to low-amplitude forcing at other frequencies. This assumption of insensitivity was first proposed over 20 years ago [1] and has since been cited throughout the literature, even though it has only ever been justified with phenomenological models, such as the forced Landau equation.

If a hydrodynamically globally unstable flame really is insensitive to forcing at other frequencies, then it should be possible to weaken thermoacoustic oscillations by detuning the frequency of the

* Corresponding author.
  E-mail address: l.li@gatescambridge.org (L.K.B. Li).

natural hydrodynamic mode from that of the natural acoustic modes. This would be very beneficial for industrial combustors.

1.1. Hydrodynamic global instability

Hydrodynamic global, or self-excited, oscillations can be found in both reacting and non-reacting flows. Examples include flickering of candle flames [2], bulging of jet diffusion flames [3], bulging of low-density jets [4], and vortex shedding in bluff-body wakes [5]. Such oscillations are termed 'hydrodynamic' because they arise from hydrodynamic mechanisms. In the above cases, for instance, they arise from inflexion points in the cross-stream profiles of axial velocity and become increasingly unstable as the density gradient steepens in the opposite direction to the velocity gradient [6].

In a jet diffusion flame, the heat release changes the density profile and hence the velocity profile through the action of buoyancy [7,8]. Crucially, the inflexion point in the shear layer just outside the flame coincides with a steep density gradient in the opposite direction to the velocity gradient, making it absolutely unstable [7]. This causes a hydrodynamic global mode, which stretches the flame and modulates its heat release in synchronisation [9].

In this paper, we test and refute the assumption that hydrodynamically self-excited flames are insensitive to forcing. We do this experimentally, by acoustically forcing a range of jet diffusion flames. We control the strength of their global instability by changing the coflow velocity and the fuel composition. For each flame, we examine the forced response over a range of frequencies (not just at the forcing frequency) and discover much richer behaviour than that which is reported in the literature. We then show that this behaviour is similar to that of a simple model: the forced van der Pol oscillator [10]. As well as providing new insight into the way acoustic oscillations interact with hydrodynamic oscillations, this paper provides a useful tool for describing and analysing such interactions.

2. Methodology

2.1. Experimental

The experiments are performed on a round coaxial injector[1] with jet diffusion flames created from mixtures of methane and nitrogen. The flames are forced sinusoidally by a loudspeaker

mounted upstream, over a range of frequencies ($7 \leqslant f_f \leqslant 35$ Hz)[2] around the natural global frequency, f_n.

The forcing amplitude, A, is measured with the two-microphone method [12]. It is defined, at the injector plane, as the amplitude of the velocity perturbation at f_f normalised by the bulk jet velocity: $A \equiv |u'_{1,f_f}|/U_1$. At each f_f, A is incrementally increased[3] to 0.90, even though lock-in (i.e. frequency entrainment or synchronisation) often occurs earlier. Lock-in is when f_n locks into f_f, leaving no sign of the natural global mode in the power spectral density (PSD). This is a qualitative change, meaning that the onset of lock-in can be found by inspecting the PSD.

The flame response is measured with a high-speed camera (Phantom V4.2) via broadband chemiluminescence at 180 frames s^{-1}. The luminosity in each frame is summed across every pixel column, resulting in a time series (five pixel rows in height) at each axial station: $I(t, x/d_1)$. In this paper, however, only one axial station, $x/d_1 = 10$, is examined. This station is chosen for three reasons: (i) it is sufficiently far downstream that the chemiluminescent emission leads to a reliable signal-to-noise ratio without saturation; (ii) it is sufficiently far downstream that the global mode (if one exists) has time to grow and interact with the forcing; but (iii) it is not so far downstream that it coincides with the location of vortex roll-up, where the strain rates can be high enough to cause local flame extinction, especially if high forcing amplitudes are used.

Two methods are used to control the strength of the hydrodynamic global instability. In the first, coflow air is added around the flame base. This reduces the shear and advects perturbations downstream, both of which weaken the instability. In the second, the relative concentrations of methane and nitrogen are changed. Reducing the methane concentration, for example, increases the stoichiometric mixture fraction. This causes the flame to shift towards the jet centreline, closer to the shear layer. The resultant changes to the density and velocity profiles are such that the flame becomes less unstable [13].

2.2. Modelling

The forced flame system is modelled with the forced van der Pol (VDP) oscillator [10]. This particular oscillator is used because it is one of the simplest nonlinear models with self-excited

---

[1] The diameter of the inner exit is $d_1 = 6$ mm and that of the outer exit is $d_2 = 30$ mm, for an annular gap of 12 mm [11].

[2] The f_f increment is 1 Hz, except when f_n is more than 0.25 Hz from an integer frequency value, in which case an additional setting, at the 0.5 Hz increment, is used.

[3] The A increment is usually 0.20, but is reduced to 0.050 around lock-in and to 0.025 if lock-in occurs for $A < 0.10$.

Table 1
Flow conditions of the six flames under investigation (293 K and 101.3 kPa). GU, globally unstable; GS, globally stable; U_2/U_1, coflow-to-jet velocity ratio; f_n, natural global frequency.

Flame		[CH$_4$]	[N$_2$]	U_2/U_1	f_n [Hz]
1	GU	1.00	0.00	0	12.5
2	GU	1.00	0.00	0.083	13.9
3	GU	0.80	0.20	0	13.0
4	GU	0.60	0.40	0	13.3
5	GU	0.60	0.40	0.083	14.7
6	GS	0.40	0.60	0	14.3[a]

[a] This is for the lightly damped global mode, which arises only with forcing. Without forcing, Flame 6 is globally stable, with two weak modes at 14.8 and 16.1 Hz.
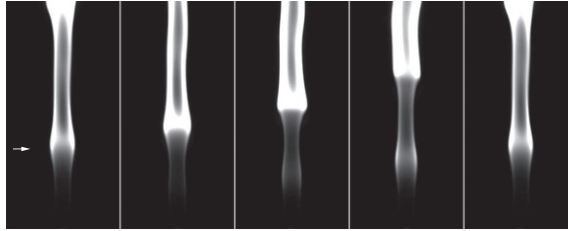

Fig. 1. Image sequence of a globally unstable flame (Flame 5) oscillating through one natural cycle. The sequence runs from left to right, and the images are separated in time by a quarter period. The white arrow indicates the axial station at which data are extracted for analysis ($x/d_1 = 10$).

solutions, an essential feature for modelling self-excited flows. As in the experiments, the forcing is external and sinusoidal:

$$\ddot{x} - \epsilon(1 - x^2)\dot{x} + \omega_n^2 x = A_{vdp}\sin(\omega_f t), \quad (1)$$

where A_{vdp} is the forcing amplitude and ω_f is its angular frequency. The feedback parameter ϵ, which controls the degree of self-excitation and nonlinear self-limitation, is fixed at an arbitrarily small value of 0.1. The natural angular frequency,[4] ω_n, is 1. Equation (1) is solved numerically using a multistep variable-order algorithm [15]. This is done for a range of forcing frequencies ($0.3 \leqslant \omega_f \leqslant 2.5$) and amplitudes in order to replicate the experimental conditions.

3. Results

3.1. Experimental

Six different flames are studied (Table 1): five globally unstable and one globally stable. For each flame, the total flow rate of the reactants is fixed at 5.0×10^{-5} m^3 s^{-1}, giving a bulk jet velocity of $U_1 = 1.77$ m s^{-1}.

---

[4] Owing to the nonlinearity, the actual frequency of the self-excited oscillations is slightly below ω_n [14]. For $\epsilon = 0.1$ (weak nonlinearity), however, this difference is negligible (<0.07%) and the oscillation frequency can be taken as $\omega \approx \omega_n$.

The globally unstable flames (Flames 1–5) all have similar natural frequencies: $12.5 \leqslant f_n \leqslant 14.7$ Hz. Figure 1 shows one of them (Flame 5) oscillating axisymmetrically through one natural cycle. The globally stable flame (Flame 6) has two natural frequencies, 14.8 and 16.1 Hz, when unforced. These, however, are replaced by a lightly damped global mode, at $f_n = 14.3$ Hz, whenever forcing is applied [11].

3.1.1. Before lock-in

First we examine the forced response before lock-in. We focus on Flame 5 because it exhibits most clearly the dynamics common to all five globally unstable flames. With the forcing frequency slightly above the natural frequency ($f_f/f_n = 1.09$), Fig. 2a shows time traces of the luminosity for five forcing amplitudes: $0.025 \leqslant A \leqslant 0.30$. For comparison, a time trace of the same signal from the same flame but without forcing is also shown (bottom). The corresponding PSD curves are shown in Fig. 2b.

The flame exhibits a rich range of dynamics:

(i) When unforced ($A = 0$), it has a global mode at a discrete natural frequency, represented in the PSD by a sharp peak at $f_n = 14.7$ Hz. There are similar, but weaker, peaks at the superharmonics, indicating that the natural varicose oscillation is not perfectly sinusoidal.

(ii) When forced at a low amplitude ($A = 0.025$), the flame responds at f_f as well as f_n. Around these two frequencies, there
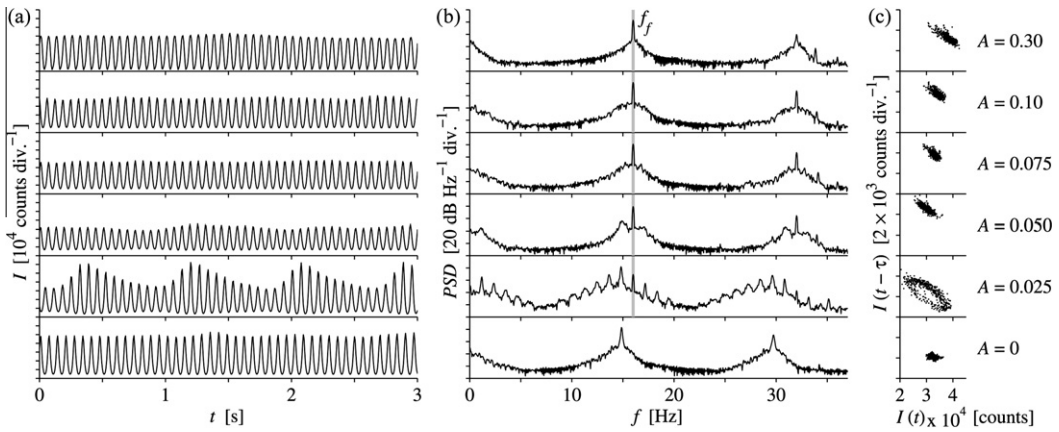
Fig. 2. (a) Time trace, (b) PSD, and (c) Poincaré map of the luminosity from Flame 5 forced at a frequency, $f_f = 16$ Hz, slightly above the natural frequency, $f_n = 14.7$ Hz: $f_f/f_n = 1.09$. The data shown are for five forcing amplitudes, $0.025 \leqslant A \leqslant 0.30$, and for the unforced case, all at $x/d_1 = 10$. The onset of lock-in occurs at $A_{loc} = 0.075$.

are multiple spectral peaks. Known as side-bands, they are caused by nonlinear (wave-triad) interactions between the natural mode and the forcing. Their presence suggests that the flame has become quasiperiodic via a Neimark – Sacker bifurcation, behaving like a typical forced oscillator before lock-in.[5] There are also spectral peaks at low frequencies, $f < 3$ Hz. Among them, the strongest corresponds to the beat frequency: $|f_f - f_n|$. In the time traces (Fig. 2a), this beating phenomenon can be seen as low-frequency (long-wavelength) modulations of the signal amplitude.

(iii) When forced at a moderate amplitude ($A = 0.050$), the flame continues to respond at both f_f and f_n, but the natural mode is noticeably weaker and its frequency is shifted slightly towards f_f.

(iv) When forced at a critical amplitude ($A = 0.075$), the flame locks into the forcing: the PSD becomes dominated by f_f and its superharmonics, with no sign of the original natural mode. The PSD of the locked-in flame resembles that of the unforced flame, except that the dominant frequency is now f_f. (Lock-in can also occur for $f_f < f_n$. For brevity, however, these results are not shown.)

The flame response at other forcing frequencies can be examined in the consolidated PSD: a contour plot of the PSD with the response frequency

Fig. 3. Forced response of Flame 5: (a) consolidated PSD for $A = 0.10$ and (b) normalised RMS luminosity for $0 \leqslant A \leqslant 0.90$, with the onset of lock-in indicated by square markers.

on the horizontal axis and f_f on the vertical axis. Figure 3a shows this for Flame 5 forced at

---

[5] In many dynamical systems, quasiperiodicity tends to arise when a self-excited oscillator is driven at a low amplitude and at a frequency that is not a rational multiple of the natural frequency (i.e. when f_f and f_n are incommensurate).
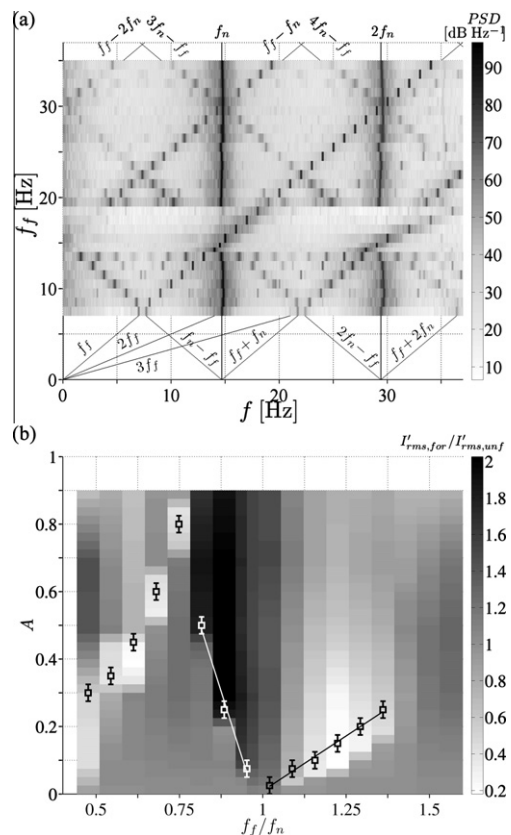
$A = 0.10$. The natural mode is indicated by a vertical stripe at f_n, which runs through all values of f_f except those to which the flame is locked in. Its second harmonic, $2f_n$, is similarly indicated. At lock-in, the forcing dominates, causing the response to consist of a diagonal stripe at $f_f = f$, with a weaker stripe at $2f_f = f$ from the second harmonic. Although not shown, the f_f band in which lock-in occurs expands vertically as A increases (Section 3.1.2).

Away from lock-in, nonlinear interactions occur between the natural mode and the forcing, giving rise to spectral peaks at low frequencies as well as around f_f and f_n – especially if the two are close. Similar interactions occur between f_f and the superharmonics of f_n. The result is that, between the vertical stripes marking f_n and its superharmonics, there are spectral peaks set in a distinctive diamond pattern.

The dynamics of the forced flame system can be understood more easily by inspecting the topology of its reconstructed phase space. Using time-delay embedding [16], we reconstruct the phase space from our high-speed camera data. We then visualise the attractors within it on the Poincaré map: a two-dimensional section through the three-dimensional phase portrait, where the system trajectory (the flame luminosity) is plotted against itself shifted by a time delay and by two time delays.[6] The Poincaré maps for Flame 5 forced at the conditions of Fig. 2a and b are shown in Fig. 2c. For clarity, these maps are cropped such that only half the section is shown.

When unforced, the phase trajectory is closed, indicating that the flame oscillates periodically at a limit cycle (of f_n). A half-section of this trajectory contains data points scattered around one blob. If the system were free of noise, the trajectory would be perfectly closed and the cropped Poincaré map would show one discrete point.

When forced at amplitudes below lock-in, the phase trajectory follows the surface of a torus. In the cropped Poincaré map, this is seen as a ring. The appearance of a torus-like structure is characteristic of quasiperiodicity – a feature corroborated by our calculations of the correlation dimension,[7] which, for intermediate Euclidean distances, show values of approximately two. For weak forcing ($A = 0.025$–0.050), the rings grow as A increases. For strong forcing ($A = 0.075$–0.30), they close to another limit cycle, this time at f_f. The final limit cycle resembles the one for the unforced flame.
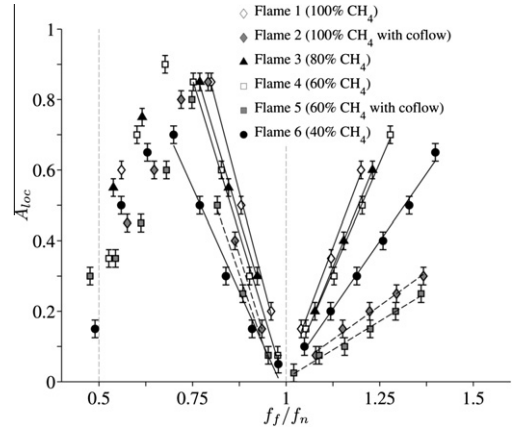
Fig. 4. Lock-in map for CH_4–N_2 jet diffusion flames. The diagonal lines through the data around $f_f/f_n = 1$ are linear fits. The error bars denote the increment with which A is varied.

These results show that a self-excited flame responds to forcing in a way that is more complicated than that which is expected from the literature. Before lock-in, the flame responds not just at its natural frequency, but also at the forcing frequency as well as at several other discrete frequencies. For combustion systems, this implies that thermoacoustic oscillations cannot be weakened simply by detuning the flame's natural frequency from the combustor's acoustic frequencies. In fact, the flame response at other frequencies may excite other acoustic modes.

3.1.2. Lock-in

Next we examine the forced response at lock-in. We start by considering the relationship between the minimum forcing amplitude required for lock-in, A_{loc}, and the normalised forcing frequency, f_f/f_n. This is shown in Fig. 4 for all six flames. The diagonal lines through the data around $f_f/f_n = 1$ are linear fits. For lock-in around the fundamental, the data at $f_f/f_n < 1$ are regressed separately from the data at $f_f/f_n > 1$. For lock-in around the subharmonic, the data are not regressed at all because the trends do not fit a linear model.

Several features are shared by all six flames. When f_f is near f_n or $f_n/2$, A_{loc} is low; otherwise it is high. Around the fundamental, A_{loc} increases in proportion to $|f_f - f_n|$, indicating a Hopf bifurcation to a global mode. This linear relationship gives rise to ∨-shaped curves, similar to those seen for other self-excited flows [4,5,21,22]. For each flame, despite the use of strong forcing, there is a limit to how far f_f can deviate from f_n before lock-in is not possible: $f_f/f_n \approx 1.2$–1.4. Around the subharmonic, the relationship between A_{loc} and $|f_f - f_n|$ is not as linear as that around the fundamental, although the overall trends are similar.

---

[6] For the optimal time delay, we use the first zero-crossing of the autocorrelation function [17].

[7] The correlation dimension is a measure of the number of degrees of freedom in a dynamical system. We estimate it using the Grassberger–Procaccia algorithm [18] as per [19,20].

Several differences exist between the six flames. As noted in Section 2.1, adding coflow weakens their global instability, which should make them more receptive to forcing, enabling lock-in to occur at lower A. This behaviour is indeed observed when Flame 1 is compared to Flame 2, and when Flame 4 is compared to Flame 5. The flames with coflow (Flames 2 and 5) lock in more readily than do their counterparts without coflow (Flames 1 and 4). This is seen not only for f_f around f_n but also for f_f on the high-frequency side of $f_n/2$.

Another way to weaken global instability is to reduce the fuel concentration. According to Fig. 4, reducing [CH_4] from 100% (Flame 1) to 80% (Flame 3) to 60% (Flame 4) has only a small effect on A_{loc}. Although the curves seem to shift downwards, the change is so small that it is within the experimental uncertainty. Reducing [CH_4] further to 40% (Flame 6), however, causes a marked decrease in the slopes of the ∨-shape. This suggests that the flame with a weak global mode (Flame 6) locks in more readily than do the flames with strong global modes (Flames 1, 3, and 4).

A final observation concerns the asymmetry of the lock-in curves about f_n: lock-in occurs more readily for $f_f/f_n > 1$ than it does for $f_f/f_n < 1$. This asymmetry is more pronounced for the flames with coflow (Flames 2 and 5) than for those without (Flames 1, 3, 4, and 6). As we will show in Section 3.2, simple model equations, such as the VDP oscillator, have symmetric lock-in curves, which means that the asymmetry is a feature of the flow, not a feature of lock-in. Theoretical work based on the Ginzburg–Landau equation suggests that when there is competition between two modes at different frequencies, one will take over and saturate nonlinearly before the other [23]. A possible explanation of asymmetric lock-in is that higher-frequency forcing produces higher peak accelerations at the flame base. In isothermal jets, higher peak accelerations have been shown to promote vortex-ring formation [24]. Forcing at higher frequencies could therefore cause toroidal vortices to roll up earlier, closer to the injector. If the vortices caused by the forcing roll up before the vortices caused by the natural global mode, they will dominate, increasing the tendency of the flame to lock in.

The fact that lock-in occurs asymmetrically suggests that there may be other asymmetries between forcing above and below f_n. To investigate this, we show in Fig. 3b contours of the response amplitude as a function of A and f_f/f_n. As before, the focus is on Flame 5 because it is representative of the globally unstable flames. The response amplitude is defined as the ratio of the root-mean-square (RMS) luminosity fluctuation with forcing to the same quantity without forcing: $I'_{rms,for}/I'_{rms,unf}$. Also shown on the figure

are selected data from Fig. 4 indicating the onset of lock-in.

As A increases for f_f/f_n slightly below 1 (Fig. 3b), the response amplitude increases above unity and saturates. As A increases for f_f/f_n slightly above 0.5 or 1, it decreases below unity, reaches a minimum near the onset of lock-in (square markers), and then increases back towards unity. As A increases for $f_f/f_n \approx 1$, it develops in a way that is between these two extremes. For $f_f/f_n > 1.36$, lock-in is not possible even with high A. Instead, over a wide band of forcing frequencies ($1.36 < f_f/f_n < 2.38$, not shown), increasing A causes a gradual rise in the response above unity, which peaks at $A \approx 0.30 - 0.50$ before decreasing.

In summary, lock-in occurs most readily for flames with weak global instability and for f_f near f_n, as expected. What was not expected, though, was that the details would depend on whether f_f is above or below f_n. When forced below f_n, the flame is more resistant to lock-in, and its oscillations at lock-in are stronger than those of the unforced flame. When forced above f_n, the flame is less resistant to lock-in, and its oscillations at lock-in are weaker than those of the unforced flame. This last finding suggests that, for thermoacoustic systems, lock-in may not be as detrimental as it is thought to be.

3.2. Modelling

For the VDP oscillator, we consider a case with the forcing frequency slightly above the natural frequency: $\omega_f/\omega_n = 1.09$. Time traces of the steady-state solution are shown in Fig. 5a for five forcing amplitudes ($0.14 \leqslant A_{vdp} \leqslant 0.40$) and for the unforced case. The corresponding PSD curves are shown in Fig. 5b. These figures are analogous to those for the flame (Fig. 2). The VDP oscillator behaves qualitatively like the flame:

(i) When unforced ($A_{vdp} = 0$), it has a dominant natural frequency, represented in the PSD by a sharp peak at $\omega_n \approx 1$. There are, however, no even harmonics, only odd ones (not shown), which are weak because the solution is nearly sinusoidal – because the cubic nonlinear term is small.

(ii) When forced at a low amplitude ($A_{vdp} = 0.14$), the VDP oscillator responds at ω_f as well as ω_n, with multiple spectral peaks around these two frequencies. Thus, like the flame, the VDP oscillator is quasi-periodic before lock-in.

(iii) When forced at a moderate amplitude ($A_{vdp} = 0.28$), the VDP oscillator continues to respond at both ω_f and ω_n. The natural mode, though, is markedly weaker and its spectral envelope is biased towards frequencies below ω_n – as indicated by the longer tail.
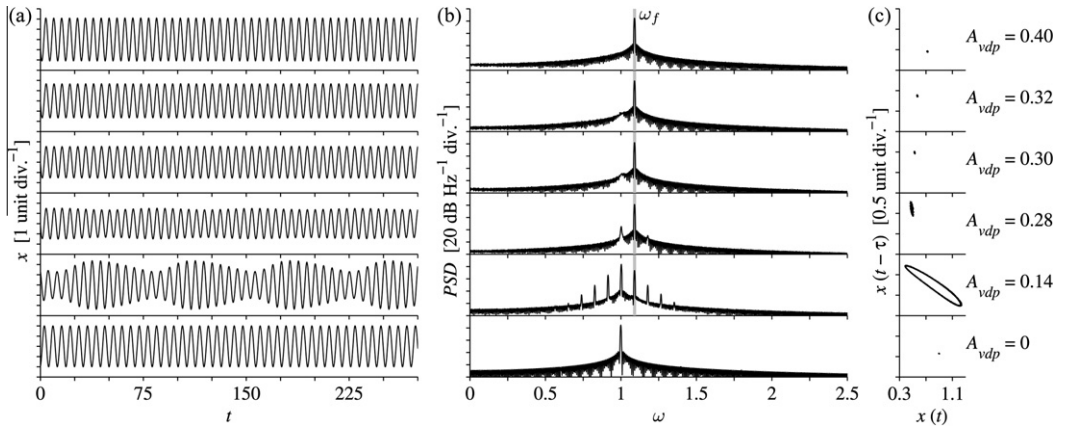
Fig. 5. (a) Time trace, (b) PSD, and (c) Poincaré map of the VDP oscillator forced at a frequency, $\omega_f = 1.09$, slightly above the natural frequency, $\omega_n = 1$: $\omega_f/\omega_n = 1.09$. The solutions shown are for five forcing amplitudes, $0.14 \leqslant A_{vdp} \leqslant 0.40$, and for the unforced case. The onset of lock-in occurs at $A_{loc} = 0.30$. This figure can be compared to Fig. 2, which is for a self-excited flame.
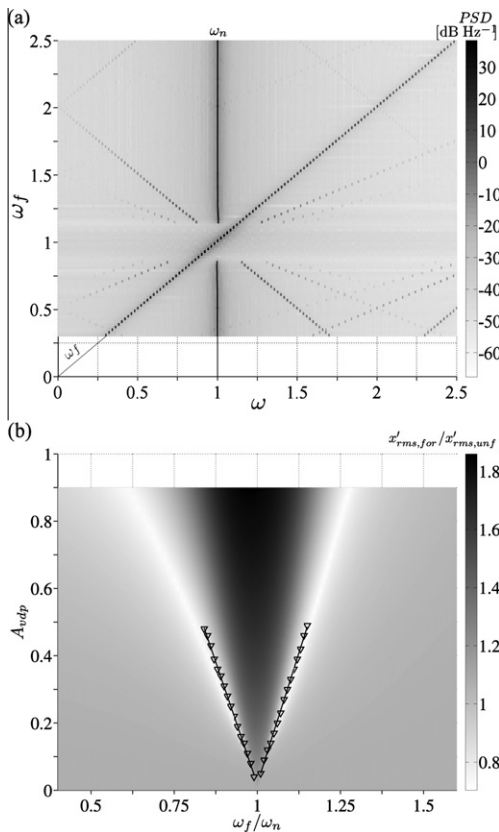

Fig. 6. Forced response of the VDP oscillator: (a) consolidated PSD for $A_{vdp} = 0.40$ and (b) normalised RMS motion for $0 \leqslant A_{vdp} \leqslant 0.90$, with the onset of lock-in indicated by triangular markers. This figure can be compared to Fig. 3, which is for a self-excited flame.

(iv) When forced at a critical amplitude ($A_{vdp} = 0.30$), the VDP oscillator locks into the forcing. This occurs because its stable equilibrium points change as the amplitude of the forcing term changes [25].

The similarities between the VDP oscillator and the flame are also apparent in the Poincaré maps (Fig. 5c). When unforced, the solution starts off as a limit cycle, but becomes quasiperiodic as A_{vdp} increases towards lock-in – as indicated by the ring-like structure and by a correlation dimension that approaches two. After lock-in, the solution converges to a new limit cycle and the phase trajectory converges to a new orbit.

The consolidated PSD (Fig. 6a) resembles the analogous plot for the flame (Fig. 3a). The vertical stripe is the response of the natural mode. When forced around ω_n, it locks into the forcing, represented by the diagonal stripe at $\omega_f = \omega$. There is, however, no diamond pattern because the VDP motion is nearly sinusoidal.

The lock-in map is shown in Fig. 6b, with A_{loc} indicated by triangular markers. The greyscale is the response amplitude, defined as the RMS of the forced solution normalised by that of the unforced solution: $x'_{rms,for}/x'_{rms,unf}$. This quantity decreases below unity as A_{vdp} increases towards lock-in, regardless of whether ω_f is above or below ω_n. At lock-in, it reaches a minimum, and its value decreases as ω_f deviates from ω_n. The lock-in curve is $\vee$ shaped and symmetric about ω_n. Although most of these features are observed in the flame, two are not: (i) the flame's response amplitude at lock-in is above (not below) unity when $f_f < f_n$; and (ii) the flame's lock-in curve is not symmetric about f_n.

4. Conclusions

We have applied acoustic forcing to a range of jet diffusion flames. These flames are self-excited by hydrodynamic resonance and thus oscillate at discrete natural frequencies. We applied the forcing around these frequencies, at varying amplitudes, and measured the response leading up to lock-in. We then modelled the system as a forced VDP oscillator.

Our results show that, contrary to some expectations, a hydrodynamically self-excited flame oscillating at one frequency is not insensitive to forcing at other frequencies. When forced at low amplitudes, it responds at both frequencies, and there is beating, indicating quasiperiodicity. When forced at high amplitudes, it locks into the forcing. The critical forcing amplitude for lock-in increases as the global instability strengthens and as the forcing frequency deviates from the natural frequency. This latter dependence is linear, giving rise to a ∨-shaped lock-in curve.

The lock-in curve has two subtle asymmetries about the natural frequency. First, a lower forcing amplitude is required for lock-in when the forcing frequency is above the natural frequency. Second, the response amplitude at lock-in is weaker than the unforced amplitude when the forcing frequency is above the natural frequency, but is stronger than it when the forcing frequency is below the natural frequency.

Many of these features can be predicted by the forced VDP oscillator. They include (i) the coexistence of the natural and forcing frequencies before lock-in; (ii) the presence of multiple spectral peaks around these competing frequencies, indicating quasiperiodicity; (iii) the occurrence of lock-in above a critical forcing amplitude; (iv) the ∨-shaped lock-in curve; and (v) the reduced response amplitude at lock-in. There are, however, some features that cannot be predicted. They include (i) the asymmetry of the forcing amplitude required for lock-in; and (ii) the asymmetry of the response amplitude at lock-in. One of our next steps is to modify the classical VDP oscillator so that it can predict both of these asymmetries.

Our results have conflicting implications for thermoacoustics. On one hand, they show that a flame's response at the forcing frequency cannot be eliminated simply by ensuring that it has a hydrodynamically self-excited mode at another frequency. In fact, the flame responds at several discrete frequencies, potentially exciting other acoustic modes in the combustor. On the other hand, our results also show that when lock-in occurs with the forcing frequency above the natural frequency, the flame oscillations are suppressed relative to the unforced case. This suggests that lock-in may not be as detrimental as it is thought to be.

References

[1] P. Huerre, P. Monkewitz, *Annu. Rev. Fluid Mech.* 22 (1990) 473–537.
[2] T. Maxworthy, *J. Fluid Mech.* 390 (1999) 297–323.
[3] M. Juniper, L. Li, J. Nichols, *Proc. Combust. Inst.* 32 (2009) 1191–1198.
[4] K. Sreenivasan, S. Raghu, D. Kyle, *Exp. Fluids* 7 (1989) 309–317.
[5] M. Provansal, C. Mathis, L. Boyer, *J. Fluid Mech.* 182 (1987) 1–22.
[6] J. Nichols, P. Schmid, J. Riley, *J. Fluid Mech.* 582 (2007) 341–376.
[7] A. Lingens, K. Neemann, J. Meyer, M. Schreiber, *Proc. Combust. Inst.* 26 (1996) 1053–1061.
[8] D. Durao, J. Whitelaw, *Proc. R. Soc. Lond. A* 338 (1974) 479–501.
[9] L. Chen, J. Seaba, W. Roquemore, L. Goss, *Proc. Combust. Inst.* 22 (1989) 677–684.
[10] B. van der Pol, J. van der Mark, *Nature* 120 (1927) 363–364.
[11] L. Li, *Forcing of Globally Unstable Jets and Flames*, Ph.D. thesis, University of Cambridge, Department of Engineering, 2011.
[12] A. Seybert, D. Ross, *J. Acoust. Soc. Am.* 61 (1977) 1362–1370.
[13] M. Füri, P. Papas, R. Rais, P. Monkewitz, *Proc. Combust. Inst.* 29 (2002) 1653–1661.
[14] D. Guicking, K. Haars, *Acustica* 73 (1991) 158–161.
[15] L. Shampine, M. Reichelt, *SIAM J. Sci. Comput.* 18 (1997) 1–22.
[16] D. Ruelle, F. Takens, *Commun. Math Phys.* 20 (1971) 167–192.
[17] H. Abarbanel, *Analysis of Observed Chaotic Data*, Springer-Verlag, New York, NY, USA, 1996.
[18] P. Grassberger, I. Procaccia, *Phys. Rev. Lett.* 50 (1983) 346–349.
[19] H. Gotoda, T. Ueda, *Proc. Combust. Inst.* 29 (2002) 1503–1509.
[20] T. Lieuwen, *J. Propul. Power* 18 (2002) 61–67.
[21] B. Bellows, A. Hreiz, T. Lieuwen, *J. Propul. Power* 24 (2008) 628–631.
[22] J. Davitian, D. Getsinger, C. Hendrickson, A. Karagozian, *J. Fluid Mech.* 661 (2010) 294–315.
[23] B. Pier, *Proc. Roy. Soc. A – Math. Phys.* 459 (2003) 1105–1115.
[24] C. Külsheimer, H. Büchner, *Combust. Flame* 131 (2002) 70–84.
[25] D. Jordan, P. Smith, *Nonlinear Ordinary Differential Equations*, 4th ed., Oxford University Press, Oxford, England, 2007.